Sub-Area Latency in a Real Time Power Network Simulator

Luis R. Linares José R. Martí

The University of British Columbia
Department of Electrical Engineering
Vancouver, B.C., Canada

Abstract

A method to exploit latency in power electric network transient simulations is proposed. The method relative accuracy and stability are explored. The network is segmented into areas which have different time responses. Latency is exploited in the resulting set of sub-networks: each of these is simulated with a possibly different integration step related to the sub-network time response characteristics.

Keywords: Real-time, simulation, EMTP, latency, multi-step rules.

1. Introduction

The use of variable-size time steps is an attractive concept in the simulation of transient phenomena. In principle, using larger time steps when the phenomenon slows down and smaller time steps when the phenomenon speeds up, computational savings can be achieved without sacrificing accuracy. This is the approach used by the well-known program SPICE [8]. The problem with this approach is how to guess, in advance, the appropriate time step size to be used for the yet unknown solution at the next time step. In our experience, in many instances these algorithms can make the wrong guess with the result of excessive time wasted or accuracy and stability problems. A better alternative to dynamically adjusted time step sizes is probably the concept of sub-circuit *latency*, that is to solve each sub-circuit with a Δt that is adequate to the sub-circuit's natural time constant. The application of this concept in connection with the solution technique in the electromagnetic transients program EMTP is discussed in this paper.

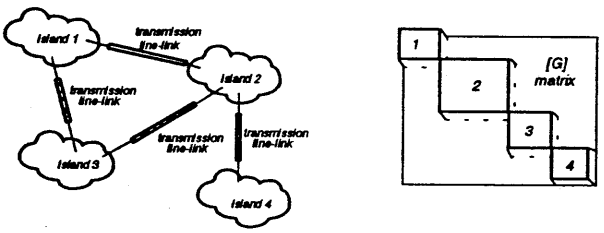

Figure 1. Topological Segmentation.

To simulate a network in the Electromagnetic Transient Program, EMTP, Eq. (1) has to be solved at each time step [3]:

$$[G][v] = [h] - [B][v_B], \qquad (1)$$

where $[G]$ is the nodal admittance matrix, $[v]$ the node voltages, $[h]$ the node injected currents, and $[v_B]$ the independent voltage sources.

Convenient node reordering techniques can convert the network nodal admittance matrix $[G]$ of Eq. (1) into a block-diagonal one, Fig. 1. The resulting non-zero blocks in $[G]$ correspond to quasi-decoupled regions in the network. An example of this approach is to use topological segmentation [1], provided by the transmission links. After this blocking procedure Eq. (1) becomes a separate set of equations, one equation for each decoupled segment, see Fig. 1.

Some of the resulting sub-networks, or areas, may have faster time response than others. In the traditional unique integration step approach, the fastest area imposes the integration step to be used by all the other areas in the system. If the system is solved using a different integration step for each area (as suggested, for example, in [6]), and the integration step is proportional to the corresponding dominant eigenvalue of the state space matrix of the sub-area, significant savings in computation time can be obtained, as illustrated in the next paragraph.

The following example is considered as a visualization example. After triangularization, the solution of a system with 1200 nodes would require approximately 1.44 million long floating point operations (i.e. multiplications and divisions). It can be estimated that the EMTP's sparsity techniques reduce this to some 35000 long flops. If that system can be broken down into 200 decoupled areas of six nodes each, the solution will need $200 \cdot 6^2 = 7200$ long flops. If one assumes, for example, that of those 200 areas, 100 of them are four times slower than the fastest one, fifty are ten times slower, 25 are 20 times slower, 25 are 25 times slower, and latency is exploited as suggested above, the solution would only need an average of

$$6^2\left(1 + \frac{25}{25} + \frac{25}{20} + \frac{50}{10} + \frac{100}{4}\right) = 1197$$

long floating point operations.

Before committing the real-time simulator to even such a

promising method, the procedure's accuracy and stability must be revised.

2. Stability of the Multi-Step Rule

Stability of the multi-step integration rule is investigated through its behaviour in the solution in the continuous time domain (CTD) of a circuit with integration (capacitor), differentiation (inductor) , and two areas with different characteristic eigenvalues; see Fig. 2.

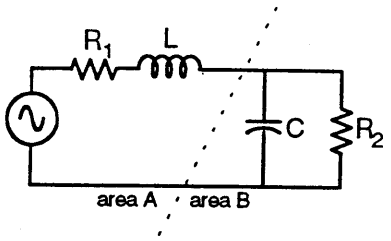

Figure 2. Simple RLC circuit with two areas.

Two areas with different time responses can be identified in the test case; namely, the RL or area A, and the RC or area B. Area B is ten times *slower* than area A. Integration step relative values have been chosen in accordance with each area characteristic time response:

$$\Delta t_A = \Delta t_{fast} = 50\mu s \tag{1a}$$

$$\Delta t_B = \Delta t_{slow} = 200\mu s \tag{1b}$$

Of the different possible approaches to consider the *latency* of area *B*, the simplest has been used in this study, i.e. to freeze *B*'s associated values between updating cycles; see Fig. 3.

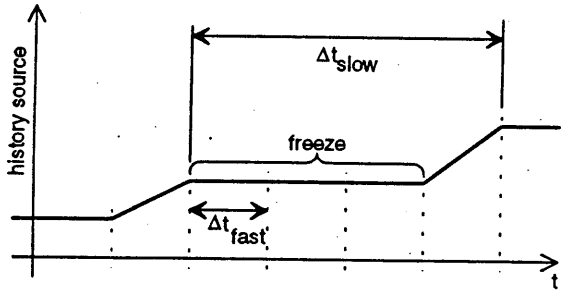

Figure 3. Freezing the latent area values.

The test case in Fig. 2, once discretized, becomes the circuit in Fig. 4, where time-areas have been separated by a dotted line. At each solution step voltages at nodes 1 and 2 (V_1, V_C) are solved for depending on whether the *slow* area is latent or not.

When the *slow* area is not latent, the associated subnetwork can be solved by Eq. (2).

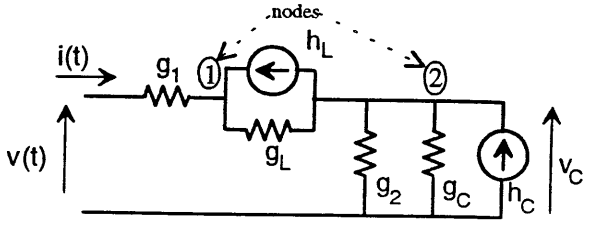

Figure 4. Discretized circuit for test case.

$$\begin{bmatrix} v_1 \\ v_C \end{bmatrix} = \underbrace{\begin{bmatrix} (g_1+g_L) & -g_L \\ -g_L & (g_2+g_L+g_C) \end{bmatrix}^{-1}}_{[A]} \begin{bmatrix} h_L+g_1 v_S \\ h_C-h_L \end{bmatrix} \tag{2}$$

When the *slow* sub-network is dormant:

$$v_1 = A_{11}(h_L+g_1 v_S) + A_{12}(h_C-h_L). \tag{3}$$

History current sources are updated according to:

$$h_C(t) = 2g_C v_C(t-\Delta t) - h_C(t-\Delta t) \tag{4a}$$

$$h_L(t) = -2g_L v_L(t-\Delta t) + h_L(t-\Delta t) \tag{4b}$$

Where:

$$g_1 = \tfrac{1}{R_1}, \quad g_2 = \tfrac{1}{R_2}. \tag{4c}$$

A unitary impulse sequence is then applied as voltage source, i.e.:

$$v[0] = 1, \quad v[n] = 0 \quad \forall n \neq 0. \tag{5}$$

The input current sequence obtained, $i_u[n]$, is the *impulse response* of the multi-step filter, see Fig. 5. The accumulated sequence is bounded; i.e.:

$$\sum_{n=0}^{\infty} i_u[n] \leq B < \infty. \tag{6}$$

This means that the multi-step filter is stable in the BIBO sense [5].

One can go one step further, and find an approximate

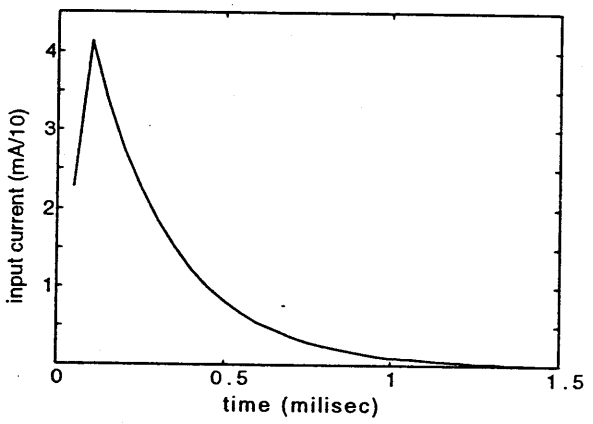

Figure 5. Impulse response of the multi-step rule.

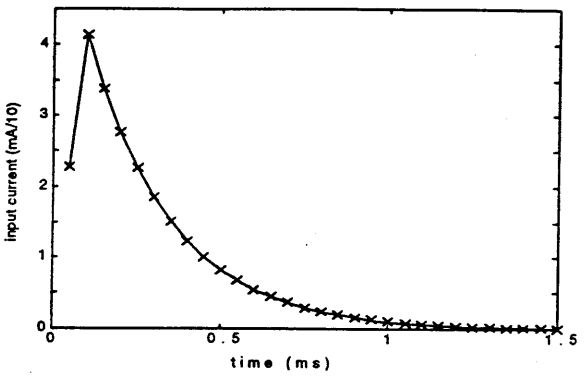

Figure 6. Superposition of impulse responses for the multi-step filter (solid line) and its *Prony* approximation.

transfer function that matches the impulse response in Fig. 5 with the *Prony* procedure [7]. The Z-domain transfer function obtained is:

$$H(z) = \frac{I(z)}{V(z)} = \frac{k(z+1)(z-0.9845)}{(z-0.9836)(z-0.8192)}, \qquad (7)$$

where k is a constant.

The match of the impulse response of this transfer function and the one in Fig. 5 can be observed in Fig. 6, where the impulse response of $H(z)$ in Eq. (7) is represented by X's superimposed on the curve in Fig. 5.

The filter is stable indeed as all its singularities are within the unitary circle, but it is critically stable [2] (zero at -1) when excited by a current source. This suggests that some adjustment like the *CDA* in [4] may be necessary across discontinuities.

3. Accuracy of the Multi-Step Rule

An integration rule performs its task with decreasing accuracy as the frequency of the signal under process approaches the Nyquist frequency. To evaluate the multi-step rule's accuracy, its frequency response is compared with that of the single-step rule.

The circuit used (integrator and differentiator) is shown in Figs. 2 and 4. This probe circuit has two time areas, as mentioned in the previous sections.

Three cases are reviewed for the frequency response characteristics, namely:

1) Area A solved with $\Delta t = 50\mu s$, and area B solved with $\Delta t = 200\ \mu s$. Multi-step rule.
2) Both areas solved with $\Delta t = 50\ \mu s$. Single-step rule with fastest integration step.
3) Both areas solved with $\Delta t = 200\ \mu s$. Single-step rule with slowest integration step.

The relative accuracy is monitored as seen through a driving port into the fastest area, that of the source in Figs. 2 and 4.

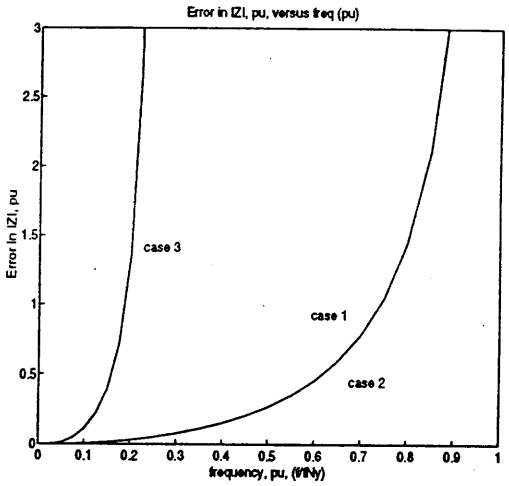

Figure 7. Frequency response of the integration rules for case (1)—dotted line—, case (2)—solid line—, and case (3) —solid line—.

a) Determining the Frequency Response

For single-step integration rules [2], it is convenient to obtain the necessary transfer function, H(z), in the Z-transform domain as seen by the rule, then, after substituting

$$z = e^{j\omega\Delta t}, \qquad (8)$$

the frequency response plots in magnitude |H(z)| and angle, *angle*(H(z)), can be drawn.

For hybrid rules such as the multi-step filter under scrutiny, a more general method can be used, as seen below.

The sampling rate or rates are set to convenient values, and kept constant during all the subsequent steps in order to anchor the Nyquist's frequency or frequencies.

Then, for a set of frequencies between zero and the

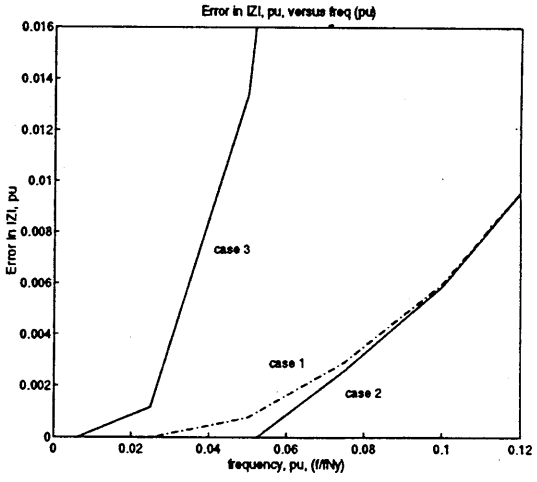

Figure 8. Detail of the characteristic frequency response for low frequencies of the integration rules for case (1)—dotted line—, case (2)—solid line—, and case (3) —solid line—.

Nyquist frequency of the fastest-area, f:

1) Apply a cosine-wave voltage source with a frequency f, as indicated in Figs. 2 and 4,
$$v(t) = \cos(2\pi f \cdot t). \quad (9)$$
2) Determine the discretized input current using the rule, $i_d(t)$, over a significant number of cycles of the source's frequency, once the initial transients have died out.
3) Put the samples of $i(t)$ obtained in (2), i.e. $i_d(t)$, through a low pass filter according to the sampling rate used in the fastest area (the one with the driving port), Δt, to reconstruct a full cycle of $i(t)$,
$$i(t) = \sum_{k=0}^{\infty} i_d(k \cdot \Delta t) \frac{\sin[(\pi/\Delta t)(t - k \cdot \Delta t)]}{(\pi/\Delta t)(t - k \cdot \Delta t)} \quad (10)$$
4) From the reconstructed cycle of the input current, obtained in (3), determine the current's amplitude, I_p, and phase shift, ϕ_I, with respect to the source signal.
5) The approximate rule-distorted driving point impedance has the magnitude $|Z_a| = 1/I_p$; and the phase shift is $\phi_{Za} = -\phi_I$.
6) Determine the exact driving point impedance at that frequency from the explicit phasor expression:
$$|Z_x(\omega)| \angle \phi_x = R(\omega) + jX(\omega) \quad (11a)$$
$$R(\omega) = R_1 + \frac{R_2}{1 + (\omega R_2 C)^2} \quad (11b)$$
$$X(\omega) = \omega \left[L - \frac{R_2^2 C}{1 + (\omega R_2 C)^2} \right] \quad (11c)$$
7) The amplitude error, in p.u., at that frequency is:
$$\varepsilon_M = 1 - \frac{|Z_a|}{|Z_x|} \quad (12a)$$
and the phase error (in units) is:
$$\varepsilon_\phi = \phi_{Z_a} - \phi_x \quad (12b)$$

b) Comparing the Frequency Responses

The frequency response characteristics obtained for cases 1, 2, and 3, described above, are shown in Fig. 7, up to the Nyquist frequency corresponding to the fastest area's integration step, which is the critical area. On this graphic, the response for the multi-step rule coincides with that of the single-step rule corresponding to the smallest integration step. Figure 8 shows an amplified view of the same graphics for very low frequencies, even at this level of magnification it can be seen that the multi-step rule is not much less accurate than the single-step rule.

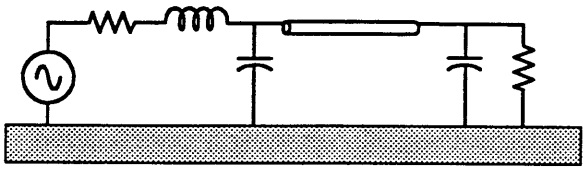

Figure 9. Simple system with a transmission link.

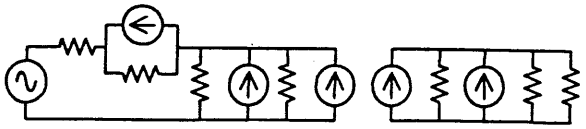

Figure 10. Discretized form of system in Fig. 9.

For higher frequencies the difference in accuracy between the multi-step and the single-step rule is of no consequence.

The single-step simulation with the larger integration step (the one corresponding to the slowest area) provided the frequency response curve shown in Figs. 7 and 8 with the label 3. It is included only for reference, but it shows that its distortion is significantly worse than that of the multi-step rule, and that it fails to include frequencies still present in the multi-step rule output and possibly of importance for the faster area.

4. Segmentation and Latency

Even if the multi-step integration rule is as stable and accurate as seen above, to incorporate it into the real-time simulator requires an answer to the question of how to break the network into areas suitable to our purpose.

The segmentation scheme that proved successful in the real-time simulator described in [1] offers a convenient arena to exploit latency by this multi-step approach.

In that topological segmentation, see Fig. 1, each transmission link sections the network into areas. For example, the system shown in Fig. 9, once discretized becomes that in Fig. 10. The decoupling effect introduced by the transmission link is evident, and the creation of two areas gives us the possibility to exploit latency.

The next step is to obtain those areas' time responses. While in coupled network equations, like the ones corresponding to the circuit in Figs. 2 and 4, to break the network into areas is rather artificial, topological segmentation produces clean-cut islands.

If each of those islands can be described in the state-space domain by an equation of the form
$$[\dot{x}] = [A][x] + [B][y], \quad (13)$$
the eigenvalues of matrix $[A]$ determine directly the time-response characteristic of that island.

5. Conclusions

Improved performance for a real-time simulator has been proposed by the exploitation of the network inherent latency. Latency is taken advantage of by a multi-step integration scheme.

The topological network segmentation scheme provided by transmission links is reviewed as an ideal case for the application of a multi-step integration method.

Work is in progress to find general techniques that may allow the further breaking down of compact subnetworks (networks with no transmission like links) into subareas of different latency.

The analysis presented in this paper shows that multi-latency integration schemes are numerically stable and their application can result in considerable savings in solution time with practically no sacrifice in solution accuracy.

6. References

[1] J.R. Martí and L.R. Linares, "*Real-Time EMTP-based transient simulation,*" IEEE Trans. on Power Systems, Vol. 9, No. 3, August 1994, pp. 1309-1317.

[2] J.R. Martí and J. Lin, "*Suppression of Numerical Oscillations in the EMTP,*" IEEE/PES 1988 Summer Meeting. Paper 88 SM 732-0, Portland, 1988.

[3] H.W. Dommel, "*Digital Computer Solution of Electromagnetic Transients in Single- and Multiphase Networks,*" IEEE Trans. on Power Apparatus and Systems, Vol. PAS-88, No. 4, 1969, pp. 388-398.

[4] J. Lin and J.R. Martí, "*Implementation of the CDA Procedure in the EMTP,*" IEEE-Power Engineering System Society, 1988 Summer Meeting, Long Beach, California, July 9-14 1989, 8 pages.

[5] A.V. Oppenheim and R.W. Schafer, "*Discrete-Time Signal Processing,*" (Book) Prentice-Hall Signal Processing Series, Ed. Prentice-Hall, Inc., New Jersey, 1989.

[6] A. Semlyen and F. De León, "*Computation of Electro-Magnetic Transients using Dual or Multiple Time Steps,*" IEEE Transactions on Power Systems, Vol. 8, No. 3, August 1993, pp. 1274-1281.

[7] T.W. Parks and C.S. Burrus, "*Digital Filter-Design,*" (Book) Ed. John Wiley & Sons, New York 1987. pp. 226-228.

[8] L.W. Nagel: "*SPICE2: A Computer Program to Simulate Semiconductor Circuits,*" Memorandum No. ERL-M520, Electronic Research Laboratory, College of Engineering, University of California, Berkeley, May 9, 1975.